ACS SyntheticBiology
Letter
Cite This: ACS Synth. Biol. 2018, 7, 1219−1228
pubs.acs.org/synthbio

Mathematical Modeling of RNA-Based Architectures for Closed Loop Control of Gene Expression

Deepak K. Agrawal,[▽,†] Xun Tang,[▽,‡] Alexandra Westbrook,[§] Ryan Marshall,[∥] Colin S. Maxwell,[¶] Julius Lucks,[#] Vincent Noireaux,[∥] Chase L. Beisel,[¶,⊥] Mary J. Dunlop,[*,†] and Elisa Franco[*,‡]

[†]Biomedical Engineering Department, Boston University, Boston, Massachusetts 02215, United States
[‡]Department of Mechanical Engineering, University of California at Riverside, Riverside, California 92521, United States
[§]Robert F. Smith School of Chemical and Biomolecular Engineering, Cornell University, Ithaca, New York 14853, United States
[∥]School of Physics and Astronomy, University of Minnesota, Minneapolis, Minnesota 55455, United States
[¶]Department of Chemical and Biomolecular Engineering, North Carolina State University, Raleigh, North Carolina 27695, United States
[⊥]Helmholtz Institute for RNA-Based Infection Research (HIRI), Josef-Schneider-Str. 2/D15, D-97080 Würzburg, Germany
[#]Department of Chemical and Biological Engineering, Northwestern University, Evanston, Illinois 60208, United States

Supporting Information

ABSTRACT: Feedback allows biological systems to control gene expression precisely and reliably, even in the presence of uncertainty, by sensing and processing environmental changes. Taking inspiration from natural architectures, synthetic biologists have engineered feedback loops to tune the dynamics and improve the robustness and predictability of gene expression. However, experimental implementations of biomolecular control systems are still far from satisfying performance specifications typically achieved by electrical or mechanical control systems. To address this gap, we present mathematical models of biomolecular controllers that enable reference tracking, disturbance rejection, and tuning of the temporal response of gene expression. These controllers employ RNA transcriptional regulators to achieve closed loop control where feedback is introduced *via* molecular sequestration. Sensitivity analysis of the models allows us to identify which parameters influence the transient and steady state response of a target gene expression process, as well as which biologically plausible parameter values enable perfect reference tracking. We quantify performance using typical control theory metrics to characterize response properties and provide clear selection guidelines for practical applications. Our results indicate that RNA regulators are well-suited for building robust and precise feedback controllers for gene expression. Additionally, our approach illustrates several quantitative methods useful for assessing the performance of biomolecular feedback control systems.

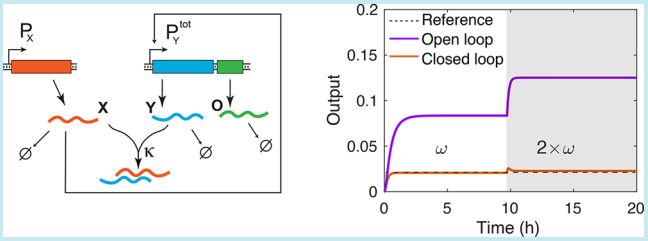

KEYWORDS: *RNA, feedback, gene expression, mathematical modeling, control, sensitivity analysis*

Cells continuously respond to their environment by producing and degrading a variety of molecules that play important roles in metabolic reactions. These reactions often require stable levels of gene expression, even in the presence of exogenous or endogenous disturbances. Feedback in native transcriptional networks can enable homeostasis and reduce variability,[1,2] and engineered negative feedback loops have been used to robustly regulate the concentration of an output species.[3−6] Yet, there are still few universal closed loop feedback architectures that have the capacity to precisely determine the dynamics and the robustness of a target gene expression process.[7,8] Biomolecular feedback systems are generally built *ad hoc*, using a limited number of orthogonal promoters and protein transcription factors, and their design is rarely portable to other processes or hosts.[9] Recent advances in RNA synthetic biology enable the construction of modular control systems that are easily adaptable to a broad range of processes.[10]

Regulatory RNAs and CRISPRi have emerged as powerful tools for constructing dynamic genetic circuits for controlling gene expression.[11−15] In particular, small transcription activating RNAs (STARs) and gRNA-dCas9 regulators are two examples of RNA based regulators that can be designed to target different genes simultaneously, and these regulators offer up to three orders of magnitude of dynamic range of operation above background.[16−19] The versatility and programmability of these emerging tools make it possible to design control systems targeting an expanding set of processes within a variety of biological hosts.

Received: January 26, 2018
Published: April 30, 2018

DOI: 10.1021/acssynbio.8b00040
ACS Synth. Biol. 2018, 7, 1219−1228

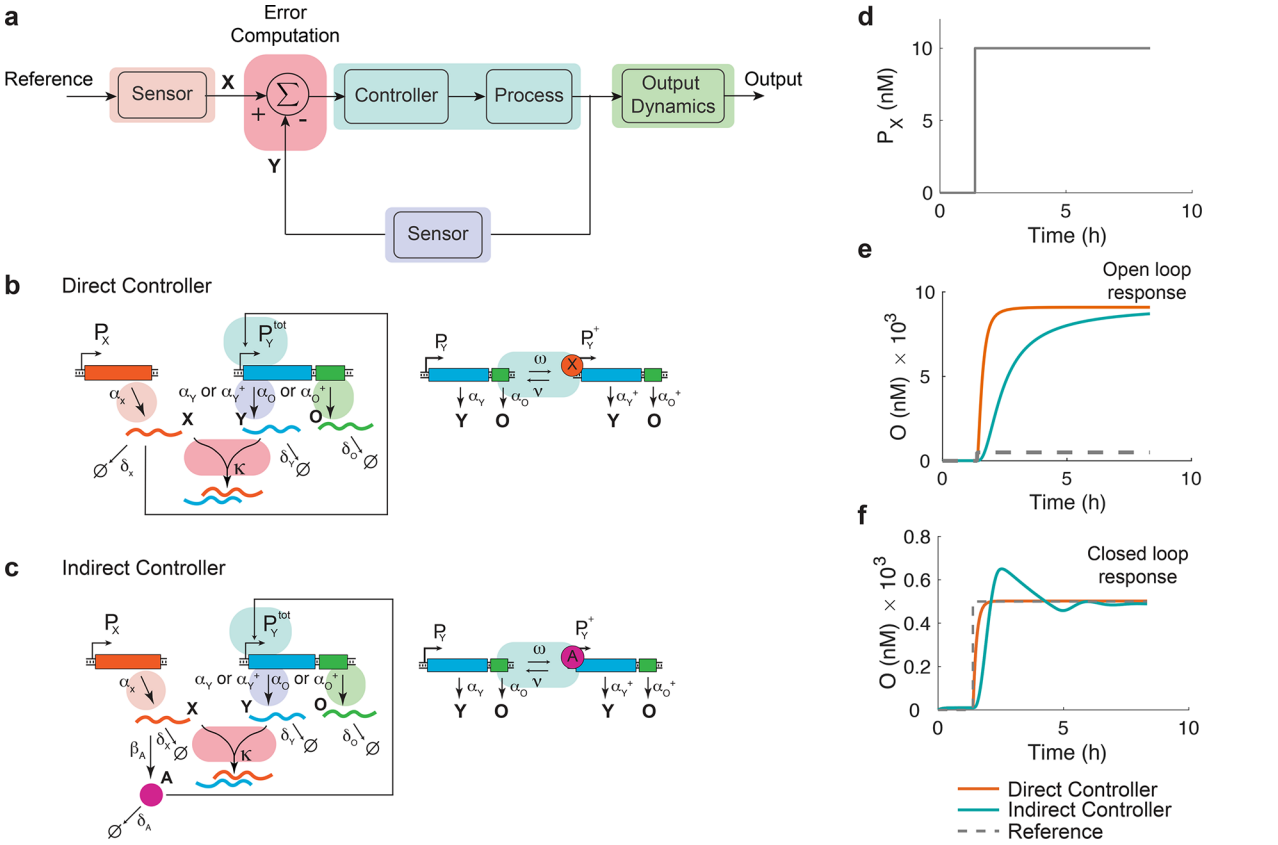

Figure 1. Closed loop controller designs. (a) Block diagram representation of the closed loop controller. (b) Direct Controller and (c) Indirect Controller designs, where the color coding corresponds to the blocks shown in (a). Each design uses RNA transcripts (X and Y) to control expression from the promoter P_Y. Error computation is achieved through a molecular sequestration reaction. The error signal controls transcriptional activation, which is performed either directly through X in the Direct Controller or through an intermediate species A in the Indirect Controller. Details on how the promoter switches from the inactive (P_Y) to active (P_Y^+) state are shown alongside. (d) Step change in P_X. Note that we define the reference as $(\alpha_O^+\alpha_X)/(\delta_O\alpha_Y^+)P_X$ (see Supplementary Note S1); therefore, this step change in P_X corresponds to a change in the reference signal from 0 to 500 nM. (e) Simulation results for the open loop and (f) closed loop controllers. Models are given in eqs 1−9, with parameters in Table 1. Initial concentrations of molecular species were set to X, Y, A, O, and P_Y^+ = 0 nM and P_Y = 20 nM unless otherwise specified.

Here, we present designs for two closed loop biomolecular controllers that employ different RNA regulation mechanisms to precisely control the expression of a target gene. Feedback is introduced *via* molecular sequestration that serves as an error computation mechanism. We compare the two regulatory schemes in their capacity to guarantee that an output species can accurately follow changes in a reference signal, even if the kinetic rates are perturbed or a disturbance is added. We develop ordinary differential equation (ODE) models of these controllers and analyze their operation through numerical and mathematical analysis considering a realistic set of parameters. We also conduct sensitivity analysis to understand the influence of parameter variability on the output dynamics when the input undergoes a step change. The two controllers work at different time scales and are compared quantitatively using traditional control theory metrics, which illustrates the trade-offs between design and performance. This computational study serves as a guide in the design of RNA-based biomolecular controllers for robust and precise regulation of gene expression. In addition, our work highlights a numerical approach to screen controller performance so that it meets specific requirements in practical applications.

RESULTS

Closed Loop RNA-Based Controller Designs. Our overall goal is to develop a closed loop biochemical controller that can precisely regulate expression of a target gene. With the controller, the output concentration (an RNA transcript) should follow a reference signal (also known as the set-point in traditional control systems).[20] The output should track the reference robustly, *i.e.*, at steady state the difference between the reference and the output should be zero following a disturbance such as perturbations of the kinetic parameters. Moreover, the controller should also be tunable to meet performance specifications that govern its transient and steady state behavior.

Our approach is to interconnect biomolecular sensors and actuators using the feedback loop architecture traditionally used in many engineering fields (Figure 1a). To achieve robust tracking, the process output is compared to a reference signal: the difference between these signals is called the error. The goal of the controller is to reduce the steady state error as much as possible, ideally to zero. The process and the reference must be measured internally using biochemical sensors, which relay information by producing the molecules X (representing the reference signal) and Y (representing the process signal); these molecules are used for error computation while avoiding depletion of the reference and process molecules. When a

DOI: 10.1021/acssynbio.8b00040
ACS Synth. Biol. 2018, 7, 1219−1228

difference between X and Y is detected (error), a corrective signal is computed by the controller block to reduce the error, *via* a negative feedback loop. The control block influences gene expression to decrease the error, leading to accurate reference tracking. The output dynamics describe the conversion from an internal signal (*e.g.*, an RNA species) to a measured external output (*e.g.*, a fluorescent reporter).

In practice, the elements of our molecular control system are genes and RNA transcripts. In our design, the concentration of plasmid or DNA encoding for X is used as the reference, and the controller regulates expression of a gene encoding for Y by influencing its promoter activity (Figure 1b). We use transcription as a signal-transduction mechanism: the constitutive promoter P_X produces an RNA signal X, and the regulated promoter P_Y produces an RNA signal Y. When activated, promoter P_Y switches to its active state P_Y^+, which transcribes signal Y at a faster rate than in the inactive state. The RNA transcripts X and Y are used for error computation, where their concentrations are compared through molecular sequestration. Once X and Y bind to each other (XY), they form a waste complex that is not involved in any other reaction in the system. The formation of complex XY is considered irreversible because the complex is degraded before it can dissociate.[21,22] As a result of the sequestration reaction, only the excess molecules of X that did not bind to Y yield an error signal that is available for control reactions. Nonsequestered X is used *directly* as an RNA transcriptional activator that regulates production of Y (Figure 1b). Thus, we name this architecture the "Direct Controller". We also considered an alternative arrangement, where an additional postsequestration reaction and intermediate species A are required, where X *indirectly* activates expression of the target gene, which we name the "Indirect Controller" (Figure 1c).

We have focused on these two designs because they describe experimentally feasible constructs. The Direct Controller models conditions where RNA species are responsible for regulatory control. For instance, X could be a small transcription activating RNA that prevents premature transcriptional termination of Y, where Y is an RNA species that can sequester X into an inert complex.[16,17] In contrast, the Indirect Controller models conditions where there is an additional regulatory step. Examples of this step include translation of X into a transcription factor A that regulates the promoter P_Y, or formation of a gRNA-dCas9 complex to activate transcription of P_Y (called CRISPR activation or CRISPRa), where X is the gRNA and A represents the gRNA-dCas9 complex.[23−29]

Effective, fast sequestration is essential in both designs for ensuring closed loop operation. If sequestration is too slow or inefficient, the process output has a limited capacity to influence expression of Y. In the limit, if the sequestration reaction is removed, the system operates without feedback (open loop). Of note, X and Y only sense the reference and output signals (Figure 1b); therefore, sequestration enables error calculation between the reference and output without affecting their dynamics, because P_X and P_Y are not depleted by sequestration. Since Y is consumed by the sequestration reaction, its concentration is not a reliable measure of the process state, *i.e.*, it exists in the sequestered complex and as a free molecule that activates transcription of promoter P_Y^+. Therefore, to measure P_Y^+ we use a reporter output species O which is coexpressed with Y and not consumed in the feedback reaction (Figures 1b and c).

Mathematical Models. Using the law of mass action, we modeled the deterministic kinetics of the Direct Controller as

$$\frac{dX}{dt} = \alpha_X P_X - \delta_X X - \kappa XY - \omega X P_Y + \nu P_Y^+ \quad (1)$$

$$\frac{dY}{dt} = \alpha_Y P_Y + \alpha_Y^+ P_Y^+ - \delta_Y Y - \kappa XY \quad (2)$$

$$\frac{dP_Y^+}{dt} = \omega X P_Y - \nu P_Y^+ \quad (3)$$

$$\frac{dO}{dt} = \alpha_O P_Y + \alpha_O^+ P_Y^+ - \delta_O O \quad (4)$$

The differential equations describe the rate of change of RNA species X and Y, the active promoter P_Y^+, and the output O. The parameters α and δ are transcription and degradation rates, with subscripts indicating the corresponding species. κ is the sequestration rate (error computation reaction). ω and ν are the association and dissociation rates that characterize binding of the transcriptional activator (X for the Direct Controller, A for the Indirect Controller) to the promoter for the gene Y. The unregulated (basal) promoter state is P_Y; the activated promoter state is P_Y^+, and due to conservation $P_Y^{tot} = P_Y + P_Y^+$ at all times. When the promoter is activated, Y and O are produced with an increased transcription rate (α^+). The basal transcription rates are α_Y and α_O, which we assume are small compared to α_Y^+ and α_O^+. α_X is the transcription rate for constitutive expression from P_X.

The dynamics of the Indirect Controller include an additional species A, which introduces a delay in the activation of P_Y. These reactions are modeled as

$$\frac{dX}{dt} = \alpha_X P_X - \delta_X X - \kappa XY \quad (5)$$

$$\frac{dY}{dt} = \alpha_Y P_Y + \alpha_Y^+ P_Y^+ - \delta_Y Y - \kappa XY \quad (6)$$

$$\frac{dA}{dt} = \beta_A X - \delta_A A - \omega A P_Y + \nu P_Y^+ \quad (7)$$

$$\frac{dP_Y^+}{dt} = \omega A P_Y - \nu P_Y^+ \quad (8)$$

$$\frac{dO}{dt} = \alpha_O P_Y + \alpha_O^+ P_Y^+ - \delta_O O \quad (9)$$

Here, β_A models the rate at which X is translated into A, or the rate at which X binds to an existing abundant species to form a complex A. Eqs 1−4 and 5−9 allow us to determine what output (O) is produced by a given input (P_X) for each control system.

In each design, the dynamics of X and Y are determined by their production rates and the rates at which they are consumed, which depend on the sequestration, degradation, and transcription rates. For the error calculation to be effective, the sequestration reaction must consume X and Y rapidly compared to other reactions that use these species, such as the degradation reaction. The adverse effect of degradation on reference tracking has been studied *in vivo* for integral controllers where cell dilution that degrades the signals can lead to error miscalculation.[30] Moreover, because X (or A in the Indirect Controller) acts as a transcriptional activator, the association rate with which the activator binds to P_Y should be

DOI: 10.1021/acssynbio.8b00040
ACS Synth. Biol. 2018, 7, 1219−1228

higher than its dissociation rate. Finally, for P_Y, the activated transcription rate needs to be significantly higher than the basal transcription rate so the error signal can be amplified to achieve production of Y and O. These design constraints must be met to achieve accurate reference tracking.

Our goal is to design closed loop controllers that can be physically implemented using RNA regulators. Therefore, for the Direct Controller we used parameter values derived from kinetic measurements of sRNA-based transcriptional regulators. For the Indirect Controller we focused on CRISPRa-based regulators, using gRNA-dCas9 to regulate target gene expression. These two classes of regulators operate at different time-scales, where sRNA rates are generally faster than those associated with CRISPRa regulation (Table 1).[17,31−34]

Table 1. Model Parameters for Each Control System[17,31−34,a]

parameters	Direct Controller (open loop)	Direct Controller (closed loop)	Indirect Controller (open loop)	Indirect Controller (closed loop)
α_X	0.1 s^{-1}	0.1 s^{-1}	0.1 s^{-1}	0.1 s^{-1}
α_Y	0.001 s^{-1}	0.001 s^{-1}	0.001 s^{-1}	0.001 s^{-1}
α_Y^+	1 s^{-1}	1 s^{-1}	1 s^{-1}	1 s^{-1}
δ_X	0.0005 s^{-1}	0.0005 s^{-1}	0.0005 s^{-1}	0.0005 s^{-1}
δ_Y	0.0005 s^{-1}	0.0005 s^{-1}	0.0005 s^{-1}	0.0005 s^{-1}
κ	0	5×10^6 M^{-1} s^{-1}	0	5×10^6 M^{-1} s^{-1}
ω	5×10^6 M^{-1} s^{-1}	5×10^6 M^{-1} s^{-1}	2.5×10^6 M^{-1} s^{-1}	2.5×10^6 M^{-1} s^{-1}
ν	1 s^{-1}	1 s^{-1}	1 s^{-1}	1 s^{-1}
β_A			0.0001 s^{-1}	0.0001 s^{-1}
δ_A			0.00005 s^{-1}	0.00005 s^{-1}
α_O	0.001 s^{-1}	0.001 s^{-1}	0.001 s^{-1}	0.001 s^{-1}
α_O^+	1 s^{-1}	1 s^{-1}	1 s^{-1}	1 s^{-1}
δ_O	0.002 s^{-1}	0.002 s^{-1}	0.002 s^{-1}	0.002 s^{-1}

[a]Note that these parameters correspond to reaction rates measured *in vitro*.

Reference Tracking with Open and Closed Loop Control. We began by verifying that the closed loop controllers with biologically feasible parameter values enable the output to track changes in the reference. To do this, we considered a step change in the input signal (P_X) from 0 to 10 nM (Figure 1d), and compared the response of the open and closed loop systems (see Methods). We define the reference signal as $(\alpha_O^+\alpha_X)/(\delta_O\alpha_Y^+)$ P_X, which is the steady state value of O for both Direct and Indirect closed loop controllers (see Supplementary Note S1 for the derivation).

We used parameters derived from the literature in the simulations (Table 1). In the absence of P_X (0 nM), expression from P_Y is very low. As P_X increases from 0 to 10 nM, the production of X increases, which in turn increases production of Y and O. In the absence of the sequestration reaction (κ = 0), the amount of X is not influenced by the concentration of Y. In this open loop case, X increases production of O, but there is no feedback to compare O (represented by Y) with the reference signal. As a result, the steady state output does not follow the reference signal (Figure 1e). The Indirect Controller behaves in a similar manner in the open loop case (Figure 1e). In contrast, in the closed loop case ($\kappa \neq 0$), the sequestration reaction determines the concentrations of free X and Y, allowing for effective calculation of the error. Therefore, in closed loop O tracks the reference signal well for both the Direct and Indirect Controllers (Figure 1f). In practice, for *in vitro* studies, a step change in P_X (from 0 to 10 nM) could be achieved by adding more DNA into the reaction mixture; for *in vivo* operation, this could be achieved through the use of an inducible promoter.

Large Variations in the Reference Signal Can Be Tracked Accurately. Although we initially considered a specific step change in P_X, accurate tracking requires that the controllers be able to follow a large range of changes in the reference signal given the same set of parameters and initial conditions. Therefore, we modeled the steady state output response of each controller for different concentration values of P_X (0, 6, 12, 18, 24, or 30 nM). For each concentration of P_X, we determined the steady state concentration of O for each closed loop controller using the parameters shown in Table 1 and a fixed initial concentration of P_Y promoter (20 nM) (see Methods). We found that both the Direct and Indirect Controllers could track the reference signal accurately (Figure 2a) such that the difference between the steady state values of reference and output were negligible (Figure 2b).

The benefit of the closed loop design became evident when we compared the open loop and closed loop systems under a wide range of initial conditions and parameter values. We tested

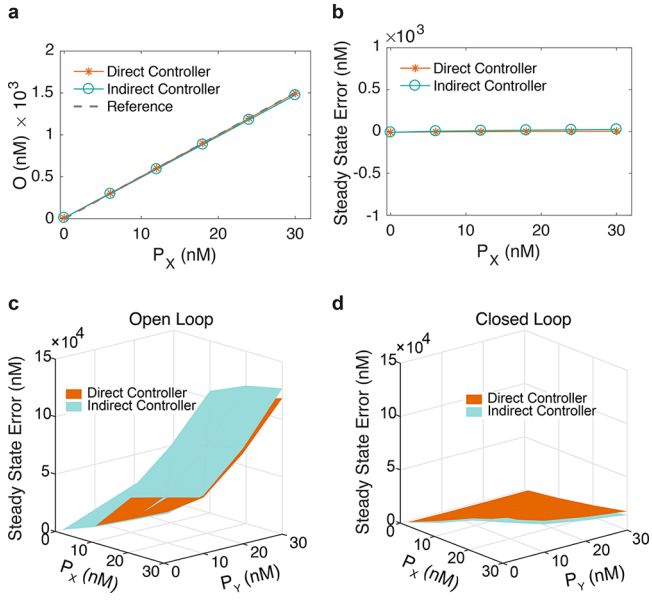

Figure 2. Output tracks the reference signal. (a) Steady state response of the Direct and Indirect Controllers at different concentrations of P_X (0−30 nM) and the corresponding (b) error between the steady state concentrations of the reference and output signal. Controllers are modeled using eqs 1−9 with parameters shown in Table 1 and initial concentration of P_Y = 20 nM. (c,d) Simulations with 10 000 sets of randomly selected parameters from within 10-fold above and below the nominal parameter values were used to simulate the two controllers for different initial P_X−P_Y combinations. Both P_X and P_Y were tested for 1, 10, 20, and 30 nM. To ensure a fair comparison, the same set of parameters was used in both controllers under each open/closed loop scenario. We simulated 10 h of data to ensure settling, and simulations that took longer than 5 h to reach the steady state were discarded from the analysis. (c) Averaged steady state error in open loop (*i.e.*, without X−Y sequestration, *i.e.*, κ = 0). (d) Averaged steady state error in closed loop (*i.e.*, with X−Y sequestration). The initial concentrations of molecular species X, Y, A, O, and P_Y^+ are 0 nM in all the simulations. For two-dimensional heat maps showing the data in (c,d) see Figure S2.

DOI: 10.1021/acssynbio.8b00040
ACS Synth. Biol. 2018, 7, 1219−1228

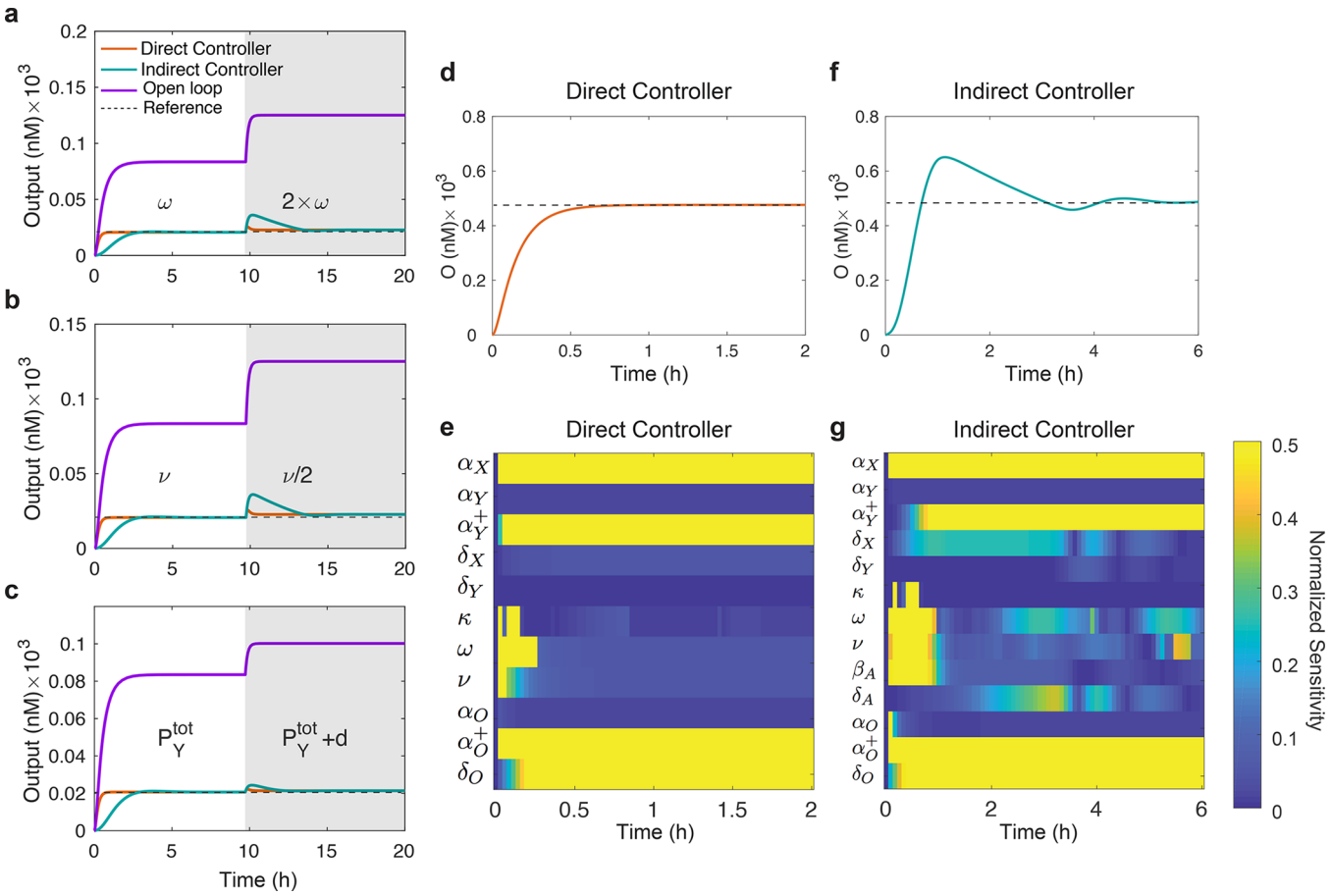

Figure 3. Robustness to disturbances and parameter sensitivity. (a–c) Output in the presence of disturbances in (a) ω, (b) ν, and (c) in the concentration of P_Y^{tot} where d = 0.1 nM. Eqs 1–9 are used to model the systems with initial concentration of X, Y, A, O, and P_Y^+ set to 0 nM while initial P_X and P_Y are both 0.5 nM. Here, the open loop response is shown for the Direct Controller, though the Indirect Controller results are similar. (d–g) Results of the sensitivity analysis: (d) Output as a function of time for the Direct Controller. (e) Normalized sensitivity matrix for the Direct Controller. (f) Output as a function of time for the Indirect Controller and (g) corresponding sensitivity matrix. The initial concentrations of P_X and P_Y are 10 and 20 nM, respectively.

initial concentrations of P_X and P_Y at 1, 10, 20, and 30 nM. To ensure that our results were not specific to a single set of parameter values, we ran 10 000 simulations with random combinations of parameters for each P_X–P_Y combination (see Methods). Simulations that did not reach a steady state after 5 h (~7% of the 10 000 simulations), for instance those with very slow transcription rates, were discarded in the analysis, as a reasonably fast settling is desirable in practical applications. Figure S1 shows a representative case where the random combination of parameters resulted in slow settling to steady state. In the rest of the cases, we calculated the average steady state error for the open loop and closed loop designs (Figure 2c,d). The addition of sequestration improved the tracking accuracy, and it reduced the average steady state error by as much as an order-of-magnitude for both the Direct and Indirect Controllers.

Interestingly, in the open loop scenario (Figure 2c), the Direct Controller had a lower steady state error than the Indirect Controller in most of the tested cases; however, the opposite was true for the closed loop (Figure 2d). One possible explanation for this phenomenon is that the intermediate species A in the Indirect Controller is produced by X in excess; therefore, it may function as an integrator of the error, which could further improve tracking accuracy when feedback is enabled. However, in both the Direct and Indirect Controllers we see uniformly low steady state errors in closed loop relative to open loop across broad ranges of parameters and initial conditions.

To understand these results further, we derived an approximate analytical expression for the steady state value of the controller output (O). In the closed loop case ($\kappa \neq 0$), *i.e.*, when sequestration dominates over degradation and the basal transcription rates are negligible compared to the activated transcription rates for O and Y species, the controller ODE models can be simplified to

$$\frac{dX}{dt} \approx \alpha_X P_X - \kappa XY \tag{10}$$

$$\frac{dY}{dt} \approx \alpha_Y^+ P_Y^+ - \kappa XY \tag{11}$$

$$\frac{dO}{dt} \approx \alpha_O^+ P_Y^+ - \delta_O O \tag{12}$$

Here, we assume that the transcriptional activation reaction is highly favorable, meaning that the dissociation rate of X (Direct Controller) or A (Indirect Controller) bound to P_Y is small ($\nu \approx 0$). At steady state, the concentration of the output can be approximated as

DOI: 10.1021/acssynbio.8b00040
ACS Synth. Biol. 2018, 7, 1219–1228

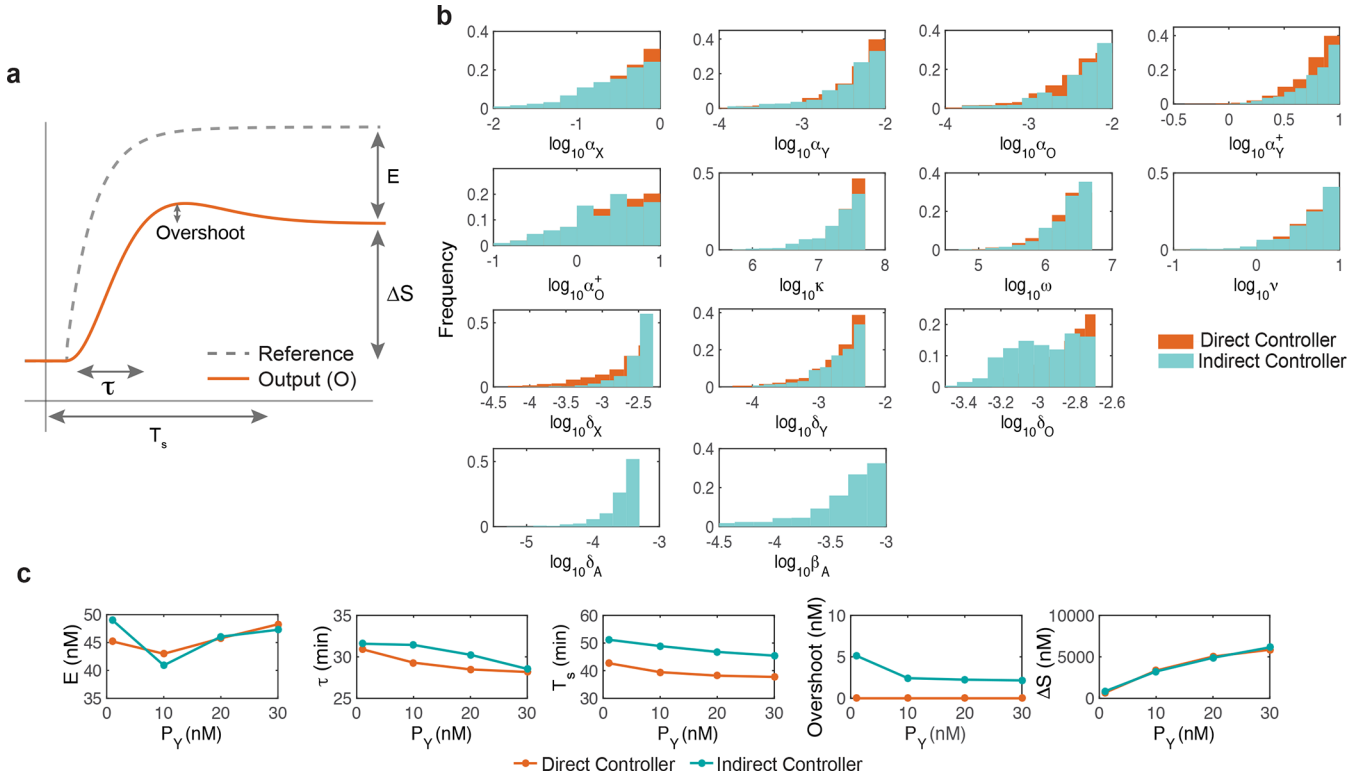

Figure 4. Performance evaluation using control theory metrics. (a) Five performance criteria are defined: the steady state error, E, is the absolute difference between the output and reference; the steady state increase, ΔS, is the difference between the steady state output after and before the step change; the Overshoot, is defined as the difference between the maximum and the steady state concentration of the output; the rise time, τ, is the time needed for the output to increase from 10% to 90% of ΔS; finally the settling time, T_s, is the first time the output settles and stays within ±5% of the steady state output concentration. A more detailed version of this figure is given in Figure S3a. (b) Parameter values for controllers that meet the performance screening criteria: steady state error less than 100 nM, rise time less than 60 min, settling time less than 120 min, overshoot less than 30 nM, and steady state increase larger than 200 nM. We used P_Y concentrations of 1, 10, 20, and 30 nM. For each P_Y concentration, we conducted 10 000 simulations with randomly selected parameter combinations. During each simulation, a step increase in P_X from 1 to 30 nM was introduced at time 10 h. The initial concentrations of molecular species X, Y, A, O, and P_Y^+ were set to 0 nM. The histograms show the values of each parameter for the controllers that met the screening criteria. Only results for P_Y = 30 nM are shown; similar histograms were obtained for other values of P_Y (Figure S3). (c) Averaged metrics over simulations that satisfy the performance criteria, over all tested P_Y concentrations. Note that the axis scale for the steady state error E is different from that in Figure 2c.

$$\bar{O} \approx \frac{\alpha_O^+}{\delta_O}\frac{\alpha_X}{\alpha_Y^+}P_X \tag{13}$$

where $\bar{O}$ denotes the steady state concentration of O given a constant input P_X (Supplementary Note S1). Note that this is the scaled version of P_X that we use as the reference signal.

Closed Loop Control Enables Disturbance Rejection. One of the potential benefits of closed loop controllers is that they can increase the robustness of the overall system by suppressing the effect of disturbances on the steady state output. To demonstrate this characteristic for the controllers we designed, we perturbed several critical reaction rates and measured the impact of the perturbation on the output. We focused on parameters that impact the steady state value of the output without altering the value of the reference signal. If the closed loop operation of the controllers is robust, at steady state the output should not change due to the perturbation.

To test this, we first perturbed kinetic rate parameters over time. In the controllers, ω is the association rate of the transcriptional activator and promoter P_Y. An increase in ω increases the affinity of the activator for the promoter, which will increase the steady state concentration of O and Y. Given a nominal ω value, we simulated the system until the output reached steady state. We then perturbed the system by increasing ω by a factor of two (see Methods). In the open loop configuration, this perturbation yields an increase in the output (Figure 3a). In contrast, in the closed loop configuration the steady state output value of both the controllers converges to the reference concentration after a transient, thereby rejecting the adverse effects of the disturbance (Figure 3a). This is because in open loop, the system lacks error computation, while in closed loop an increase in Y sequesters X, reducing production of O and Y. We also considered a temporal perturbation in ν, the dissociation rate between the activator and promoter. When we reduced ν by a factor of 2 we observed that the closed loop controllers were able to reject the effect of this perturbation on the output signal (Figure 3b).

In practical settings, promoter concentration can vary significantly, such as due to fluctuations in plasmid copy number.[35] Therefore, we also tested disturbances that influence the biochemical species P_Y^{tot} to verify that the ability to reject disturbances is not limited to perturbations in the model parameters. In each controller, the active promoter P_Y^+ produces O and Y species with an increased transcription rate relative to P_Y. Y is used to compute the error. Therefore, we hypothesized that each controller should be able to reject disturbances in P_Y^{tot} when operating in closed loop. To test this, we added a disturbance to P_Y^{tot} after the system reached

DOI: 10.1021/acssynbio.8b00040
ACS Synth. Biol. 2018, 7, 1219−1228

steady state and observed that in closed loop, the output converged to the original reference signal, as desired (Figure 3c). To test the effect of perturbations experimentally, regulatory competitors could be added to change the association (ω) and dissociation (ν) rates over time, or P_Y^{tot} could be modified in the reaction through the use of inducible promoters. We note that disturbance rejection is only possible for perturbations that do not explicitly impact the steady state output parameters, which are those present in eq 13.

Direct and Indirect Controllers Demonstrate Similar Parameter Sensitivity. Next, we determined how all model parameters govern the transient and steady state response of the controller output. For this purpose, we performed sensitivity analysis to determine how changes in the model parameters affect the dynamics of the system. We calculated the time-dependent sensitivity coefficient matrix to measure how sensitive the output is with respect to each parameter over time (see Methods).[36,37]

We conducted this analysis for each controller using the nominal parameters (Table 1), and the results for the output sensitivity are shown in Figures 3d−g. Coefficients with a high value indicate that variations in the associated parameter cause a significant change in the transient and steady state response of the output. Note that the coefficients of the normalized sensitivity matrix depend on time. We found that, for each controller, only the transient response of the output is highly sensitive to the sequestration rate (κ) and the activation parameters (ω and ν); in contrast, the steady state value of the output depends on the parameters in eq 13—a result that agrees with our analytical approximation.

Quantifying Controller Performance with Control-Theory Metrics. For a comprehensive understanding of the temporal response characteristics of the controllers, we introduced step changes in P_X ranging from 1 to 30 nM as before, and we evaluated the controller performance based on five performance criteria that are typically used in control theory (Figure 4a). Specifically, we measured the steady state error E, rise time τ, settling time T_s, Overshoot, and steady state increase ΔS.[38] Using these criteria, we compared the controllers over a range of different initial P_Y concentrations. As before, to ensure our results were not specific to particular reaction rates, we ran 10 000 simulations with random combinations of parameters for each set of P_X and P_Y initial conditions.

As an example, we specified a set of desired performance criteria designed to achieve low steady state error, fast rise time and settling time, a sizable steady state increase, and low overshoot. Specifically, we set $E \leq 100$ nM, $\tau \leq 60$ min, $T_s \leq 120$ min, Overshoot ≤ 30 nM, and $\Delta S \geq 200$ nM. We performed 10 000 simulations for each set of initial P_Y concentrations (1, 10, 20, and 30 nM), and selected the parameter combinations for which the solution satisfied the user-specified screening criteria. Figure 4b shows histograms of the parameters—11 parameters for the Direct Controller and 13 parameters for the Indirect Controller—yielding closed loop performance that met the design specifications. For this set of specifications, we found that 10% of the tested combinations of the Direct Controller met the criteria, while 5% of the Indirect Controller values achieved similar performance. The overlap between histograms, observed for all 11 parameters that the controllers have in common, confirms that the two controllers have similar performance, even though the Indirect Controller meets the performance specifications in a smaller fraction of the parameter space. For simplicity, only results obtained for P_Y = 30 nM are summarized in Figure 4b, and these results are similar for other P_Y concentrations (Figure S3).

The differences between the two controllers became more noticeable when we compared their averaged performance in each of the five criteria (Figure 4c). While both controllers had similar behavior in terms of steady state error (E), rise time (τ), and steady state increase (ΔS), the addition of the intermediate species in the Indirect Controller caused increased overshoot in response to the step change, which also led to a slower settling time T_s, as compared to the Direct Controller. The reason for this overshoot is that the intermediate species A accumulates the difference between X and Y over time before activating transcription from the P_Y promoter. These results can be used to inform synthetic controller designs, and will depend on the user-defined performance metrics selected.

DISCUSSION

In this computational study, we have shown how RNA transcriptional regulators can be used to construct closed loop biomolecular controllers that use molecular sequestration for effective and robust control of gene expression. Previous models using molecular sequestration have been proposed for closed loop controllers[6] that operate using sigma and antisigma factors. Here, we describe two sequestration-based architectures tailored to model realistic transcriptional controllers that use RNA. With well-defined techniques from control systems theory, we have demonstrated that the controllers can not only track reference signals accurately over a wide range of conditions, they can also reject perturbations introduced to the biochemical species and due to disturbances in kinetic parameters. Comparisons between the open loop and closed loop configurations illustrate the advantages of using a sequestration reaction for error computation in both controller architectures. In the absence of effective sequestration, such as when degradation dominates over the sequestration reaction, controllers have limited ability to track the reference signal and reject disturbances (Figure S4). However, we show that for biologically feasible parameters with strong sequestration, the Direct and Indirect Controller architectures perform similarly, as shown by the results of our sensitivity analysis and the controllers capacity to meet performance specifications, suggesting that this sequestration-based approach is viable for realistic biosynthetic implementations.

One of the critical design requirements we identified is that the sequestration reaction needs to dominate over the degradation reaction. The RNA−RNA binding rate (*e.g.*, sequestration rate between X and Y), is typically in the order of 10^6 M^{-1} s^{-1}.[39] RNA degradation rates can vary widely depending on the species.[40] In order to reduce the degradation rate, stabilizing sequences could be added to slow the degradation of RNA.[41] Simultaneously, the sequestration rate can be increased by adding additional complementary sequences between the two RNAs.[42]

Our Direct Controller architecture is tailored to model sRNA regulators, while the Indirect Controller can capture the dynamics of gRNA-dCas9 regulators for CRISPRa. This distinction is necessary because these two classes of regulators use different mechanisms to control gene expression. An sRNA activator (such as STAR molecules)[13,16] regulates transcriptional elongation through RNA−RNA binding, while the gRNA-dCas9 complex can regulate transcription by either binding to the promoter region of the gene to control transcription initiation, or to the gene itself to regulate

DOI: 10.1021/acssynbio.8b00040
ACS Synth. Biol. 2018, 7, 1219−1228

transcriptional elongation.[29,43−45] Furthermore, these models represent the coarse-grained behavior of the controllers and ignore processes such as RNA maturation[32] and cell dilution;[27] in the future it would be interesting to extend upon this work to include these effects. Although our models neglect detailed mechanistic processes, they demonstrate the overall feasibility of these feedback designs. Given that the Direct and Indirect controllers exhibit similar performance, our results suggest that different RNA-based regulatory mechanisms can be employed to achieve robust biological control.

In our analysis, we used an RNA transcript O as a reporter to measure the output of the closed loop system. While this can be accomplished in practice using fluorescent aptamers,[46] it is more common to use fluorescent proteins as reporters of gene expression.[47] This explicit readout mechanism requires additional translation reactions to convert the RNA transcript O into a fluorescent protein such as GFP. We considered this alternative for the Direct Controller architecture in the open and closed loop configurations by explicitly modeling the GFP output. Consistent with our previous results, we found that GFP output can follow the reference signal well in the closed loop configuration (Figure S5).

Overall, we have demonstrated that these new RNA-based controllers can enable accurate reference tracking over a broad range of inputs. Further, the designs are robust to disturbances and can meet user-specified performance criteria, such as requirements on the response time or overshoot. These controllers could be used for a wide variety of applications. Examples include precisely regulating processes involved in metabolic engineering such as microbial biofuel production,[3] in therapeutics to regulate drug delivery, or for controlling the production of antimicrobial peptides. The relative simplicity of these designs suggests that RNA-based closed loop controllers could be used within larger, more complex networks to improve robustness and performance.

METHODS

To determine the response of each controller for a given set of parameters, we numerically integrated ODE models (eqs 1−4 for the Direct Controller and eqs 5−9 for the Indirect Controller) using the MATLAB ode23s function. Initial conditions for each molecular species are described in the figure captions, and the values of reaction parameters are shown in Table 1. To determine the steady state response of the output (Figure 2a,b), simulations were conducted for 10 h for each value of P_X and the end point of O was taken to be the steady state value. For plots shown in Figures 2c,d, and 4, to generate the 10 000 combinations of kinetic parameters, each parameter was randomly sampled from a uniform distribution from an interval bounded by a lower bound of 0.1× the nominal value and an upper bound of 10× the nominal value given in Table 1. In the perturbation plots (Figure 3a−c), the response of each controller was first determined for the nominal parameters (shown in Table 1), and when the output reached the steady state, a specific disturbance was added as described in the figure.

To determine the output sensitivity of each parameter, we calculated the sensitivity coefficient matrix over time ($s_{i,j}$), which is defined as[48]

$$s_{i,j}(t) = \frac{\partial y_i}{\partial p_j} \tag{14}$$

where y_i is a molecular species and p_j is a reaction parameter where the subscript i corresponds to a particular species and the subscript j to a particular parameter in system. In our study, y_i is O and p_j can be any parameters shown in Table 1. $\mathbf{y}$ represents a general ODE model and can be expressed as

$$\frac{d\mathbf{y}}{dt} = f(\mathbf{y}, \mathbf{p}, t) \tag{15}$$

Here, $\mathbf{y}$ and $\mathbf{p}$ are the vectors of all the species and parameters, respectively. To calculate $s_{i,j}$, we use a sensitivity differential equation expressed as

$$\frac{ds_{i,j}}{dt} = \frac{\partial \mathbf{f}}{\partial \mathbf{y}} s_{i,j} + \frac{\partial \mathbf{f}}{\partial p_j} \tag{16}$$

Eq 16 is solved numerically to calculate $s_{i,j}$ for each parameter and the normalized values of $s_{i,j}$ ($\bar{s}_{i,j}$) are reported in Figure 3e,g using

$$\bar{s}_{i,j} = \frac{\partial y_i / y_i}{\partial p_j / p_j} \tag{17}$$

ASSOCIATED CONTENT

Supporting Information

The Supporting Information is available free of charge on the ACS Publications website at DOI: 10.1021/acssynbio.8b00040.

Note on steady state analysis and supplementary figures (PDF)

AUTHOR INFORMATION

Corresponding Authors

*E-mail: mjdunlop@bu.edu.

*E-mail: efranco@engr.ucr.edu.

ORCID

Julius Lucks: 0000-0002-0619-6505

Vincent Noireaux: 0000-0002-5213-273X

Mary J. Dunlop: 0000-0002-9261-8216

Elisa Franco: 0000-0003-1103-2668

Author Contributions

[▽]DKA and XT contributed equally to this work.

Notes

The authors declare no competing financial interest.

ACKNOWLEDGMENTS

The authors thank James Chappell and Hamid Ossareh for helpful discussions. This work was supported by the Defense Advanced Research Projects Agency (Contract HR0011-16-C-01-34).

REFERENCES

(1) Del Vecchio, D., and Murray, R. M. (2015) *Biomolecular Feedback Systems*, Princeton University Press.

(2) Alon, U. (2006) *An Introduction to Systems Biology: Design Principles of Biological Circuits*, CRC Press.

(3) Dunlop, M. J., Keasling, J. D., and Mukhopadhyay, A. (2010) A model for improving microbial biofuel production using a synthetic feedback loop. *Systems and Synthetic Biology* 4 (2), 95−104.

(4) Cuba Samaniego, C., Giordano, G., Kim, J., Blanchini, F., and Franco, E. (2016) Molecular titration promotes oscillations and bistability in minimal network models with monomeric regulators. *ACS Synth. Biol.* 5 (4), 321−333.

DOI: 10.1021/acssynbio.8b00040
ACS Synth. Biol. 2018, 7, 1219−1228

(5) Ma, W., Trusina, A., El-Samad, H., Lim, W. A., and Tang, C. (2009) Defining network topologies that can achieve biochemical adaptation. *Cell 138* (4), 760−773.
(6) Briat, C., Gupta, A., and Khammash, M. (2016) Antithetic integral feedback ensures robust perfect adaptation in noisy biomolecular networks. *Cell Systems 2* (1), 15−26.
(7) Briat, C., Zechner, C., and Khammash, M. (2016) Design of a synthetic integral feedback circuit: dynamic analysis and DNA implementation. *ACS Synth. Biol. 5* (10), 1108−1116.
(8) Oishi, K., and Klavins, E. (2011) Biomolecular implementation of linear I/O systems. *IET Syst. Biol. 5* (4), 252−260.
(9) Cardinale, S., and Arkin, P. A. (2012) Contextualizing context for synthetic biology − identifying causes of failures of synthetic biological systems. *Biotechnol. J. 7* (7), 856−866.
(10) Del Vecchino, D., Abdullah, H., Qian, Y., and Collins, J. J. (2017) A blueprint for a synthetic genetic feedback controller to reprogram cell fate. *Cell Systems 4* (1), 109−120.
(11) Waters, L. S., and Storz, G. (2009) Regulatory RNAs in bacteria. *Cell 136* (4), 615−628.
(12) McKeague, M., Wong, R., and Smolke, C. (2016) Opportunities in the design and application of RNA for gene expression control. *Nucleic Acids Res. 44* (7), 2987−2999.
(13) Lucks, J., Lei, Q., Mutalik, V., Wang, D., and Arkin, A. (2011) Versatile RNA-sensing transcriptional regulators for engineering genetic networks. *Proc. Natl. Acad. Sci. U. S. A. 108* (21), 8617−8622.
(14) Dominguez, A. A., Lim, W. A., and Qi, L. S. (2016) Beyond editing: repurposing CRISPR-Cas9 for precision genome regulation and interrogation. *Nat. Rev. Mol. Cell Biol. 17* (1), 5−15.
(15) Luo, M. L., Leenay, R. T., and Beisel, C. L. (2016) Current and future prospects for CRISPR-based tools in bacteria. *Biotechnol. Bioeng. 113* (5), 930−943.
(16) Chappell, J., Takahashi, M. K., and Lucks, J. B. (2015) Creating small transcription activating RNAs. *Nat. Chem. Biol. 11* (3), 214−220.
(17) Westbrook, A. M., and Lucks, J. B. (2017) Achieving large dynamic range control of gene expression with a compact RNA transcription−translation regulator. *Nucleic Acids Res. 45* (9), 5614−5624.
(18) Thakore, P. I., D'Ippolito, A. M., Song, L., Safi, A., Shivakumar, N. K., Kabadi, A. M., Reddy, T. E., Crawford, G. E., and Gersbach, C. A. (2015) Highly specific epigenome editing by CRISPR-Cas9 repressors for silencing of distal regulatory elements. *Nat. Methods 12* (12), 1143−1149.
(19) Briner, A. E., Donohoue, P. D., Gomaa, A. A., Selle, K., Slorach, E. M., Nye, C. H., Haurwitz, R. E., Beisel, C. L., May, A. P., and Barrangou, R. (2014) Guide RNA functional modules direct Cas9 activity and orthogonality. *Mol. Cell 56* (2), 333−339.
(20) Åström, K. J., and Hägglund, T. (1995) *PID Controllers: Theory, Design, And Tuning*, 2nd ed., Instrument Society of America, Research Triangle Park, NC.
(21) Levine, E., Zhang, Z., Kuhlman, T., and Hwa, T. (2007) Quantitative characteristics of gene regulation by small RNA. *PLoS Biol. 5* (9), e229.
(22) Mehta, P., Goyal, S., and Wingreen, N. S. (2008) A quantitative comparison of sRNA-based and protein-based gene regulation. *Mol. Syst. Biol. 4* (1), 221.
(23) Konermann, S., Brigham, M. D., Trevino, A. E., Joung, J., Abudayyeh, O. O., Barcena, C., Hsu, P. D., Habib, N., Gootenberg, J. S., Nishimasu, H., Nureki, O., and Zhang, F. (2014) Genome-scale transcriptional activation by an engineered CRISPR-Cas9 complex. *Nature 517*, 583−588.
(24) Perez-Pinera, P., Kocak, D. D., Vockley, C. M., Adler, A. F., Kabadi, A. M., Polstein, L. R., Thakore, P. I., Glass, K. A., Ousterout, D. G., Leong, K. W., Guilak, F., Crawford, G. E., Reddy, T. E., and Gersbach, C. A. (2013) RNA-guided gene activation by CRISPR-Cas9-based transcription factors. *Nat. Methods 10* (10), 973−976.
(25) Bikard, D., Jiang, W., Samai, P., Hochschild, A., Zhang, F., and Marraffini, L. A. (2013) Programmable repression and activation of bacterial gene expression using an engineered CRISPR-Cas system. *Nucleic Acids Res. 41* (15), 7429−7437.
(26) Maeder, M. L., Linder, S. J., Cascio, V. M., Fu, Y., Ho, Q. H., and Joung, J. K. (2013) CRISPR RNA-guided activation of endogenous human genes. *Nat. Methods 10* (10), 977−979.
(27) Chappell, J., Westbrook, A., Verosloff, M., and Lucks, J. B. (2017) Computational design of small transcription activating RNAs for versatile and dynamic gene regulation. *Nat. Commun. 8* (1), 1051.
(28) Lee, Y. J., Kim, S.-J., and Moon, T. S. (2018) Multilevel Regulation of Bacterial Gene Expression with the Combined STAR and Antisense RNA System. *ACS Synth. Biol. 7*, 853.
(29) Marshall, R., Maxwell, C. S., Collins, S. P., Jacobsen, T., Luo, M. L., Begemann, M. B., Gray, B. N., January, E., Singer, A., He, Y., Beisel, C. L., and Noireaux, V. (2018) Rapid and scalable characterization of CRISPR technologies using an E. coli. Cell-free transcription-translation system. *Mol. Cell 69* (1), 146−157.
(30) Qian, Y., and Del Vecchio, D. (2017) Realizing "Integral Control" In Living Cells: How To Overcome Leaky Integration Due To Dilution? *bioRxiv*, 141051.
(31) Siegal-Gaskins, D., Tuza, Z. A., Kim, J., Noireaux, V., and Murray, R. M. (2014) Gene circuit performance characterization and resource usage in a cell-free "breadboard. *ACS Synth. Biol. 3* (6), 416−425.
(32) Garamella, J., Marshall, R., Rustad, M., and Noireaux, V. (2016) The all E. coli TX-TL Toolbox 2.0: a platform for cell-free synthetic biology. *ACS Synth. Biol. 5* (4), 344−355.
(33) Qi, L. S., Larson, M. H., Gilbert, L. A., Doudna, J. A., Weissman, J. S., Arkin, A. P., and Lim, W. A. (2013) Repurposing CRISPR as an RNA-guided platform for sequence-specific control of gene expression. *Cell 152* (5), 1173−1183.
(34) Mekler, V., Minakhin, L., Semenova, E., Kuznedelov, K., and Severinov, K. (2016) Kinetics of the CRISPR-Cas9 effector complex assembly and the role of 3′-terminal segment of guide RNA. *Nucleic Acids Res. 44* (6), 2837−2845.
(35) Paulsson, J., and Ehrenberg, M. (2001) Noise in a minimal regulatory network: plasmid copy number control. *Q. Rev. Biophys. 34* (1), 1.
(36) Hu, C. Y., Varner, J. D., and Lucks, J. B. (2015) Generating effective models and parameters for RNA genetic circuits. *ACS Synth. Biol. 4* (8), 914−926.
(37) Yao, K. Z., Shaw, B. M., Kou, B., McAuley, K. B., and Bacon, D. (2003) Modeling ethylene/butene copolymerization with multi-site catalysts: parameter estimability and experimental design. *Polym. React. Eng. 11* (3), 563−588.
(38) Ogata, K. (2009) *Modern Control Engineering*, 5th ed., p 55, Prentice Hall, Upper Saddle River, NJ.
(39) Brantl, S., and Wagner, E. G. H. (2000) Antisense RNA-mediated transcriptional attenuation: an in vitro study of plasmid pT181. *Mol. Microbiol. 35* (6), 1469−1482.
(40) Schwalb, B., Michel, M., Zacher, B., Frühauf, K., Demel, C., Tresch, A., Gagneur, J., and Cramer, P. (2016) TT-seq maps the human transient transcriptome. *Science 352* (6290), 1225−1228.
(41) Carrier, T. A., and Keasling, J. (1999) Library of synthetic 5′ secondary structures to manipulate mRNA stability in Escherichia coli. *Biotechnology progress 15* (1), 58−64.
(42) Franco, E., Giordano, G., Forsberg, P.-O., and Murray, R. M. (2014) Negative autoregulation matches production and demand in synthetic transcriptional networks. *ACS Synth. Biol. 3* (8), 589−599.
(43) Mali, P., Esvelt, K. M., and Church, G. M. (2013) Cas9 as a versatile tool for engineering biology. *Nat. Methods 10* (10), 957−963.
(44) Mathelier, A., Fornes, O., Arenillas, D. J., Chen, C.-y., Denay, G., Lee, J., Shi, W., Shyr, C., Tan, G., and Worsley-Hunt, R. (2016) JASPAR 2016: a major expansion and update of the open-access database of transcription factor binding profiles. *Nucleic Acids Res. 44* (D1), D110−D115.
(45) Zalatan, J. G., Lee, M. E., Almeida, R., Gilbert, L. A., Whitehead, E. H., La Russa, M., Tsai, J. C., Weissman, J. S., Dueber, J. E., and Qi, L. S. (2015) Engineering complex synthetic transcriptional programs with CRISPR RNA scaffolds. *Cell 160* (1), 339−350.
(46) Paige, J. S., Wu, K. Y., and Jaffrey, S. R. (2011) RNA mimics of green fluorescent protein. *Science 333* (6042), 642−646.

DOI: 10.1021/acssynbio.8b00040
ACS Synth. Biol. 2018, 7, 1219−1228

(47) Cormack, B. P., Valdivia, R. H., and Falkow, S. (1996) FACS-optimized mutants of the green fluorescent protein (GFP). *Gene 173* (1), 33−38.
(48) Beck, J. V., and Arnold, K. J. (1977) *Parameter Estimation in Engineering and Science*, John Wiley & Sons Inc.

DOI: 10.1021/acssynbio.8b00040
ACS Synth. Biol. 2018, 7, 1219−1228

Supplementary Information

Mathematical modeling of RNA-based architectures for closed loop control of gene expression

Deepak K. Agrawal[§,‡], Xun Tang[§,†], Alexandra Westbrook[Γ], Ryan Marshall[Ξ], Colin S. Maxwell[¶], Julius Lucks[£], Vincent Noireaux[Ξ], Chase L. Beisel[¶,€], Mary J. Dunlop[*,‡], and Elisa Franco[*,†]

[‡]Biomedical Engineering Department, Boston University, Boston, MA 02215, United States
[†]Department of Mechanical Engineering, University of California at Riverside, Riverside, CA 92521, United States
[Γ]Robert F. Smith School of Chemical and Biomolecular Engineering, Cornell University, Ithaca, NY 14853, United States
[Ξ]School of Physics and Astronomy, University of Minnesota, Minneapolis, MN 55455, United States
[¶]Department of Chemical and Biomolecular Engineering, North Carolina State University, Raleigh, NC 27695, United States
[€]Helmholtz Institute for RNA-based Infection Research (HIRI), Josef-Schneider-Str. 2 / D15, D-97080 Würzburg, Germany
[£]Department of Chemical and Biological Engineering, Northwestern University, Evanston, IL 60208, United States

*Email: efranco@engr.ucr.edu, mjdunlop@bu.edu.

Supplementary Note 1: Steady state analysis

In order to determine an approximate steady state expression for O, we assume that at steady state $\kappa X \gg \delta_Y$, $\kappa Y \gg \delta_X$, $\omega X \gg \nu$, $\alpha_O^+ \gg \alpha_O$, $\alpha_Y^+ \gg \alpha_Y$, and that the transcriptional activation reaction is highly favorable. Under these assumptions, the dynamics of the P_Y^+ and A species are fast, allowing us to simplify the ODE models of the Direct Controller and the Indirect Controller (Eqns. (1-4) and Eqns. (5-9) in the main text) to:

$$\frac{dX}{dt} \approx \alpha_X P_X - \kappa XY \tag{S1}$$

$$\frac{dY}{dt} \approx \alpha_Y^+ P_Y^+ - \kappa XY \tag{S2}$$

$$\frac{dO}{dt} \approx \alpha_O^+ P_Y^+ - \delta_O O \tag{S3}$$

We can determine the steady state expression of the different species by equating the derivatives of in Eqns. (S1-S3) to zero:

$$\bar{X} \approx \frac{\alpha_X P_X}{\kappa \bar{Y}} \tag{S4}$$

$$\bar{Y} \approx \frac{\alpha_Y^+ \bar{P_Y^+}}{\kappa \bar{X}} \tag{S5}$$

$$\bar{O} \approx \frac{\alpha_O^+}{\delta_O} \bar{P_Y^+} \tag{S6}$$

where bar ($^-$) denotes the steady state concentration values. Using Eqns. (S4) and (S5), we can expresses the steady state value of $\bar{P_Y^+}$ as:

$$\bar{P_Y^+} \approx \frac{\alpha_X P_X}{\alpha_Y^+} \tag{S7}$$

Replacing Eqn. (S7) in Eqn. (S6), leads to

$$\bar{O} \approx \frac{\alpha_O^+}{\delta_O} \frac{\alpha_X P_X}{\alpha_Y^+} \tag{S8}$$

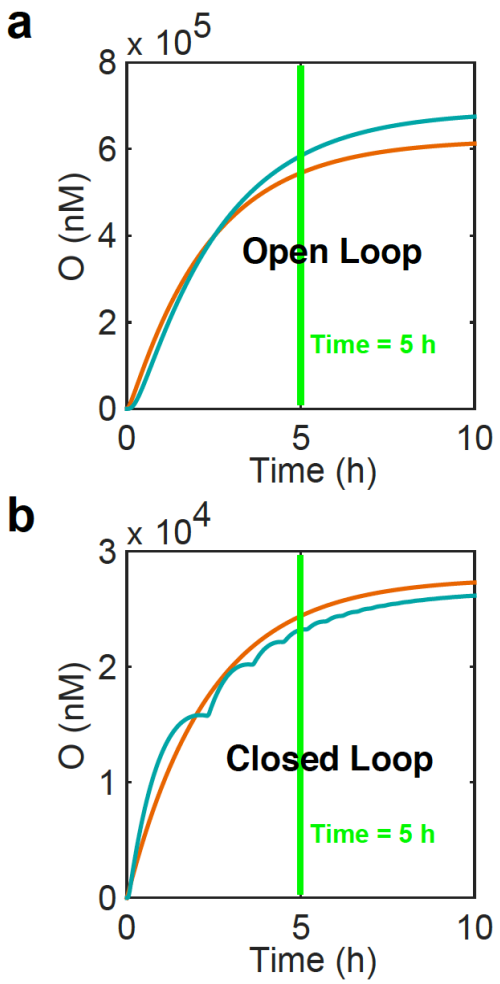

Parameters	Values
α_X	0.3568 s^{-1}
α_Y	0.0047 s^{-1}
α_Y^+	9.6276 s^{-1}
δ_X	0.0009 s^{-1}
δ_Y	0.00005 s^{-1}
κ	0 / 3.35× 10^7 M^{-1} s^{-1}
ω	3.92 × 10^6 M^{-1} s^{-1}
ν	2.40 s^{-1}
β_A	N/A / 0.00052
δ_A	N/A / 0.00016
α_O	0.0025 s^{-1}
α_O^+	8.5460 s^{-1}
δ_O	0.00012 s^{-1}

Figure S1: Representative example of the 7% of trajectories that did not reach steady state after 5 hours of simulation time in the study in Fig. 2c-d of the main text, with: (a) Open loop simulations for both the Direct and Indirect controllers, and (b) Closed loop simulations for both the Direct and Indirect controllers, using parameters given in the table. Note that $\kappa = 0$ was used in the open loop, β_A and δ_A are not applicable in the Direct Controller. All the simulations were conducted with an initial concentration of $P_Y = 10$ nM and $P_x = 10$ nM.

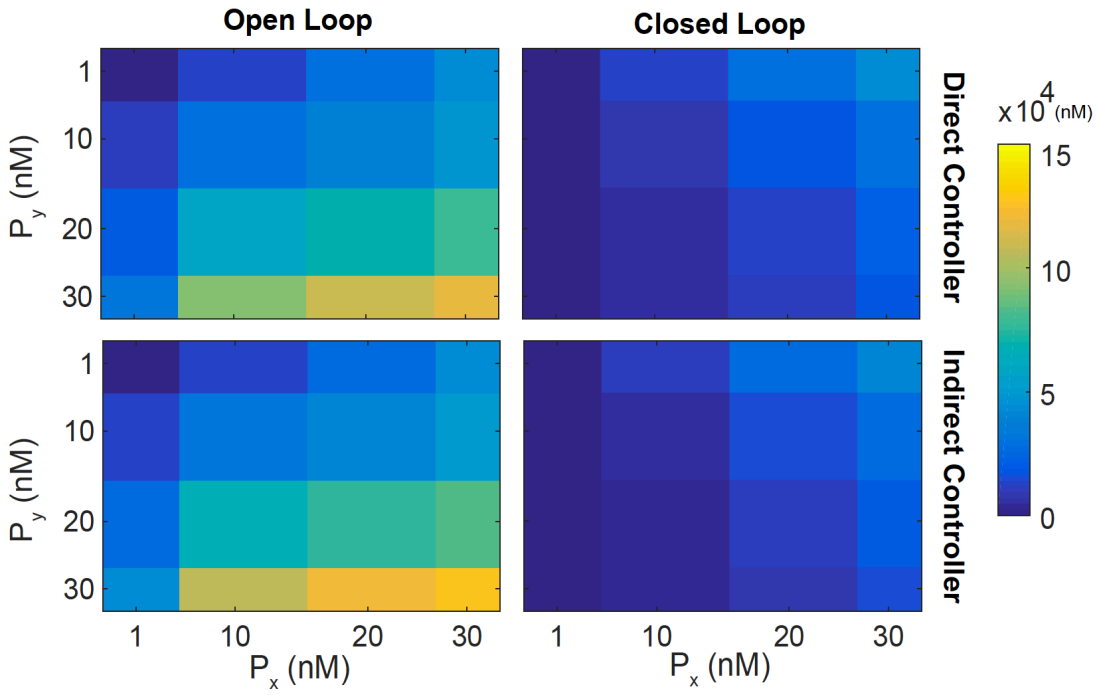

Figure S2: Two-dimensional view of of Fig. 2c-d from the main text reveals a complementary point-to-point comparison between the open and closed loop for the two controllers, in the P_y-P_x phase plane. Color bar indicates the steady state error in nM.

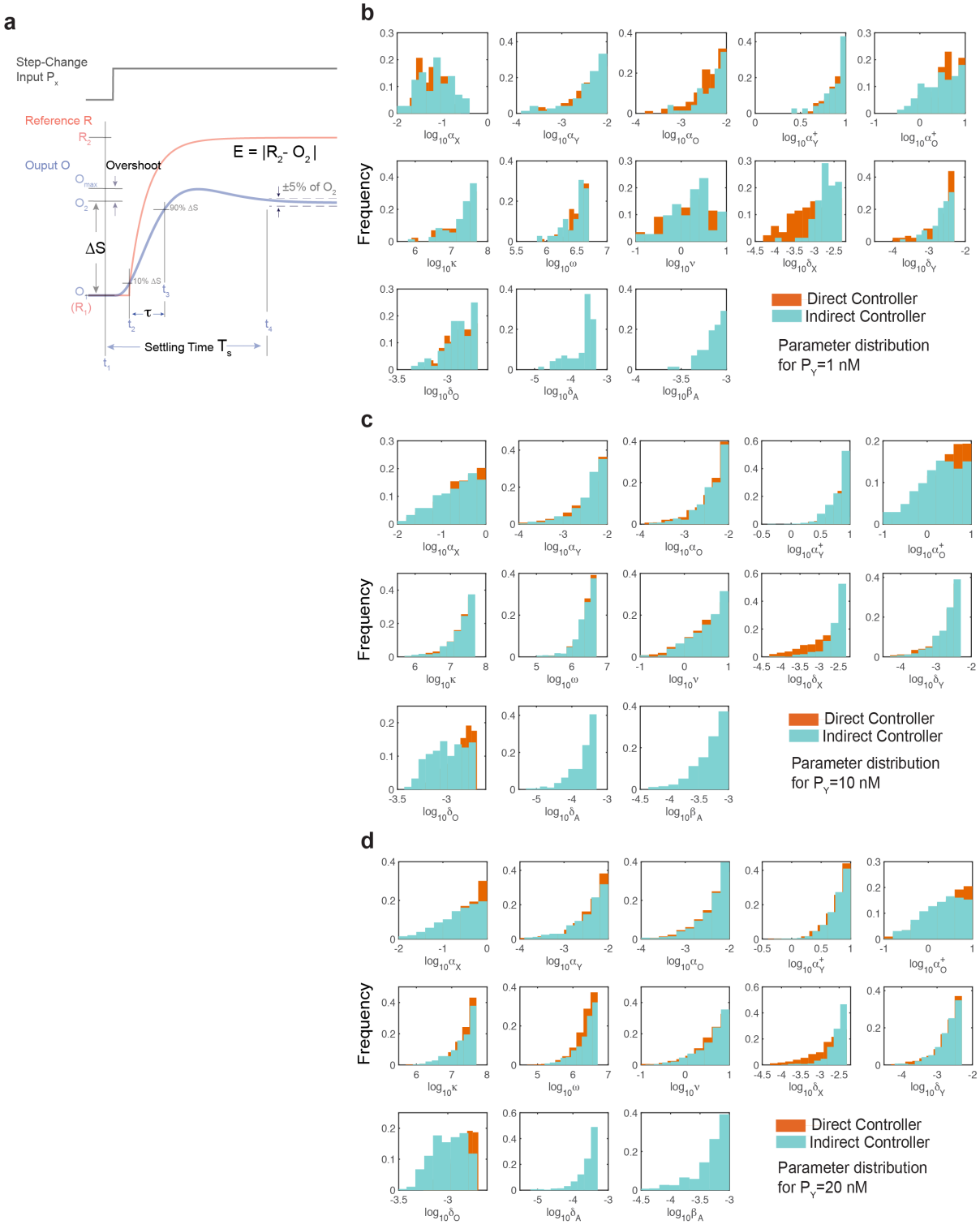

Figure S3: (a) Detailed definition of the five performance criteria: steady state error, *E*; steady state increase, *ΔS*; Overshoot; rise time, τ; and settling time, T_s. Parameter distributions for the Direct and Indirect Controllers to achieve the performance metrics specified in the main text, with initial P_Y concentrations of (b) 1 nM, (c) 10 nM, and (d) 20 nM. We introduced a

step change from 1 to 30 nM in P_x at time 10 hours. Each simulation lasted for a total of 20 hours to ensure steady state convergence. Note that as in Fig. 4 in the main text, all parameters have similar distributions between the two controllers. For P_Y of 1 nM, ~1% of the tested combinations for both controllers satisfied the criteria; for P_Y of 10 and 20 nM, ~10% of the tested combinations for the Direct Controller satisfy the criteria, while only ~5% for the Indirect Controller met the same criteria.

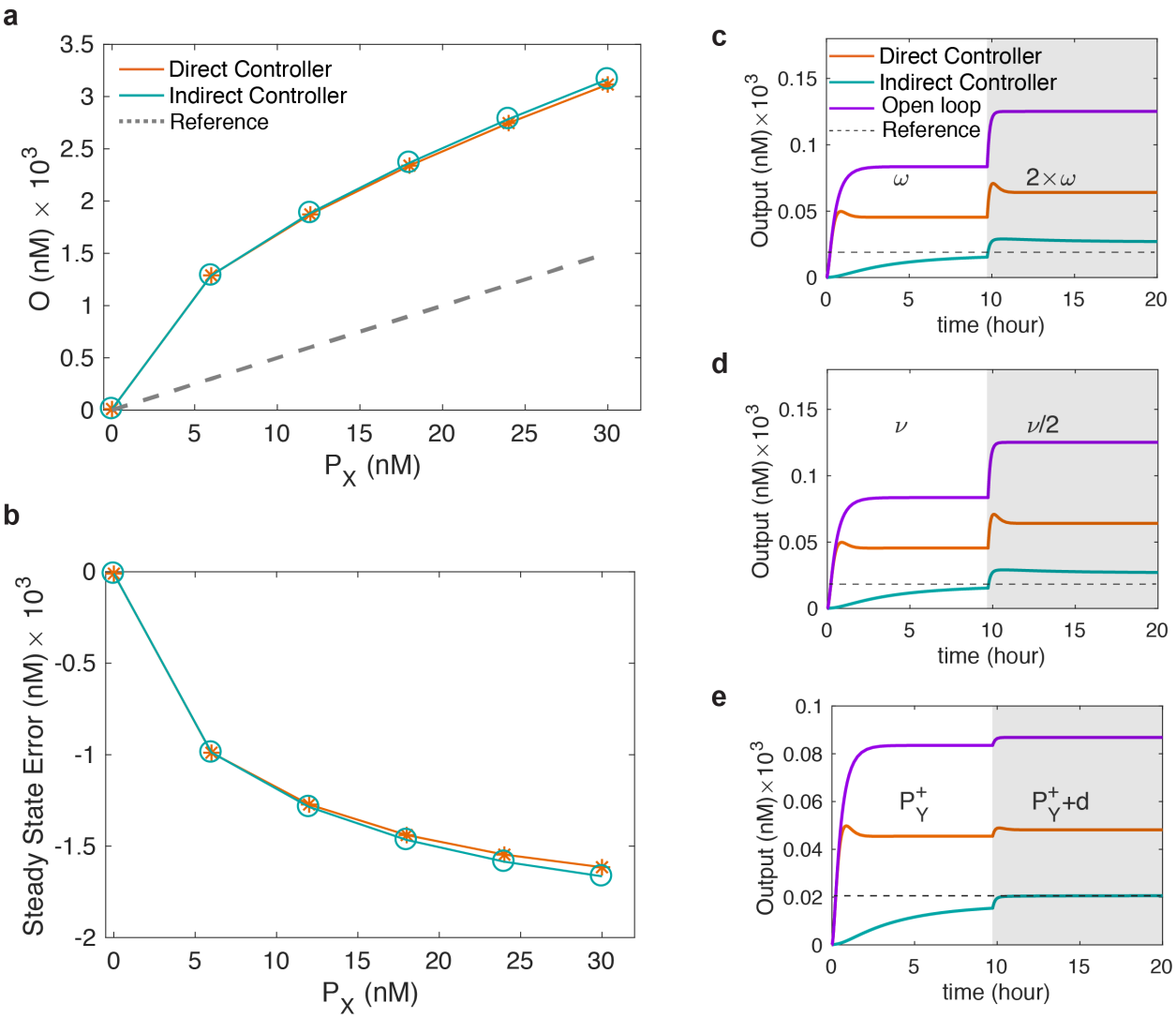

Figure S4: Controllers perform poorly when the sequestration reaction is ineffective. (a) Steady state response of the Direct and Indirect Controllers at different concentrations of P_X (0 - 30 nM) and (b) the corresponding steady state error between the steady state concentration values of the reference signal and output signal. For closed loop operation with ineffective sequestration we use $\kappa = 5 \times 10^3$ $M^{-1}s^{-1}$, a value at which the error computation is not effective. Equations (1-9) are used to model the systems with initial concentrations of X, Y, A, O, and P_Y^+ set to 0 nM while P_Y is 20 nM. Other reaction parameters are shown in Table 1. (c-e) Output in the presence of disturbances in (c) ω, (d) ν, and (e) in the concentration of P_Y^+ where d = 40 nM. The initial concentrations of P_X and P_Y are 0.5 nM. Here, the open loop response is shown for the Direct Controller.

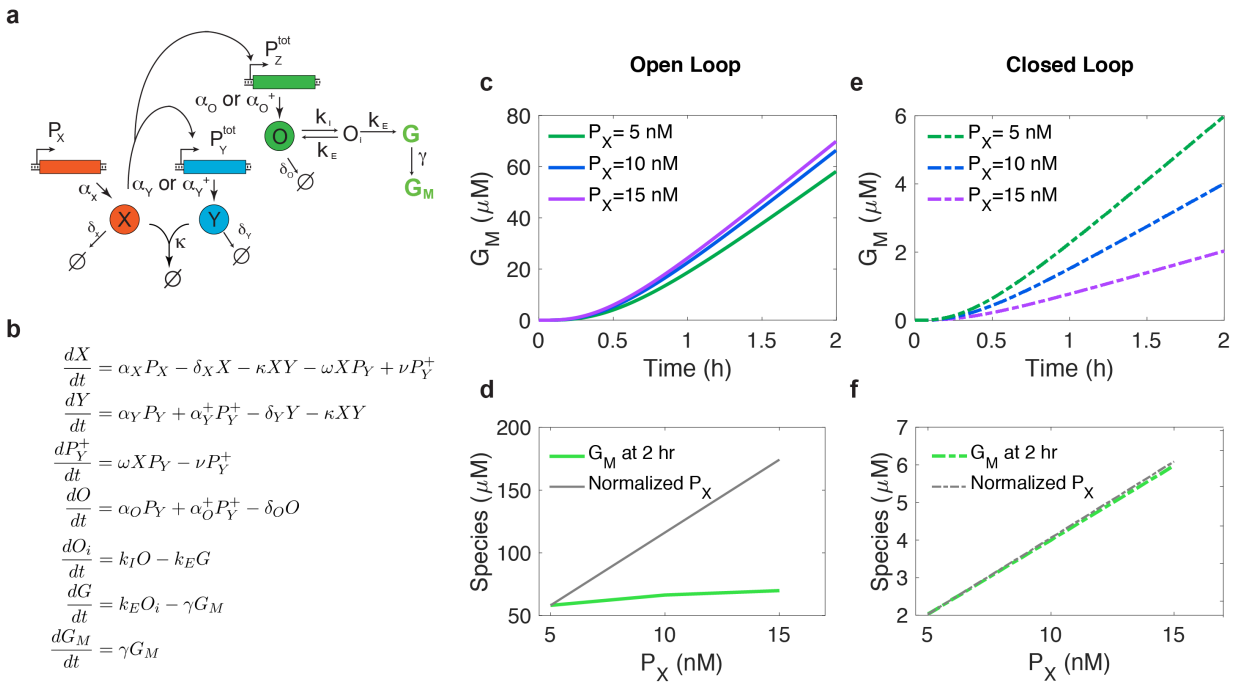

$$\frac{dX}{dt} = \alpha_X P_X - \delta_X X - \kappa XY - \omega X P_Y + \nu P_Y^+$$
$$\frac{dY}{dt} = \alpha_Y P_Y + \alpha_Y^+ P_Y^+ - \delta_Y Y - \kappa XY$$
$$\frac{dP_Y^+}{dt} = \omega X P_Y - \nu P_Y^+$$
$$\frac{dO}{dt} = \alpha_O P_Y + \alpha_O^+ P_Y^+ - \delta_O O$$
$$\frac{dO_i}{dt} = k_I O - k_E G$$
$$\frac{dG}{dt} = k_E O_i - \gamma G_M$$
$$\frac{dG_M}{dt} = \gamma G_M$$

Figure S5: Explicitly modeling GFP output for the Direct Controller. (a) Additional reactions are added into the model so that O is translated into a fluorescent protein (G_M).[1] Here k_i and k_E are the translation initiation and elongation rates and γ is the maturation rate for G_M. O_i is the translationally initiated mRNA of the GFP protein, G is the immature G_M. (b) ODE model of the reaction network shown in (a). (c-f) Increases in P_X lead to increases in GFP expression (G_M) when the controller is operating either in the (c, d) open loop configuration or in the (e, f) closed loop configuration. However, in the open loop configuration the changes in G_M expression (d) are not proportional to changes in the P_X value, while in the (f) closed loop configuration they are. Here, the P_X concentration is normalized with respect to the G_M value when P_X = 5 nM at 2 hours. In the simulation k_i= 0.0014 s^{-1}, k_E= 0.001 s^{-1}, and γ=0.2 s^{-1}; other rates are listed in Table 1 in the main text.

REFERENCES

1. Hu, C. Y.; Varner, J. D.; Lucks, J. B., Generating effective models and parameters for RNA genetic circuits. ACS synthetic biology 2015, 4 (8), 914-926.